Robust Convergence Technique against Multilevel Random Effects in Stochastic Modeling of Wearable Antennas' Far-Field

Jinxin Du, Ruimeng Wang, Christophe Roblin, *Member, IEEE*, Xue-Xia Yang, *Senior Member, IEEE*, *Bin Han, Senior Member, IEEE*

***Abstract*—Stochastic modeling is widely employed to characterize uncertainty propagation in fluctuating wearable antenna systems. A major challenge that hinders the convergence of stochastic models is the multilevel random effects on antenna's far-field caused by random disturbances, which exacerbate the already difficult inherent issue tied to high dimensionality and nonlinearity. This paper proposes to separately model the "*global*" random effect depending mainly on frequency, and the "*fine*" random effect depending mainly on antenna's directional characteristics. The "decoupling" of *global* and *fine* effects is obtained by separately modeling the reflection coefficient S_{11} and a newly defined "desensitized" far-field, which is insensitive to detuning (or mismatch) phenomena. A "centering" technique based on cross-correlation is used to reduce the sensibility of S_{11} to the randomness. The whole strategy significantly accelerates the convergence of the modeling process, resulting in a "bi-level" surrogate model that exhibits enhanced robustness and accuracy. Comparative tests on a flexible textile patch antenna demonstrate that the proposed technique can reduce modeling costs by 57% while maintaining the same level of model accuracy. The proposed solution could expand the application of stochastic modeling to a broader spectrum of antenna characterization and optimization.**

***Index Terms*— Wearable antennas, stochastic modeling, multilevel random effects, convergence, robustness.**

I. Introduction

Flexible antennas are highly promising candidates for wearable applications thanks to their attractive features such as being low profile, conformable, unobtrusive, ease to integrate, and cost-effective [1-2]. These antennas commonly operate in fluctuating environments and are subject to stochastic uncertainties caused by multiple sources of randomness, including intrinsic deformations like bending, torsion, crumpling, and external disturbances like humidity, temperature, body proximity effects, etc. Such uncertainties have a substantial impact on the real-time performance of wireless body area networks (WBAN), and should be quantitatively characterized prior to implementation. With the trend of antenna miniaturization, arraying, and integration, the boundary between antennas and their surrounding environment becomes less distinct, resulting in the amplification of random effects. Stochastic modeling has emerged as a good approach for quantifying the propagation of uncertainties, treating the antenna and its immediate environment as a unified entity.

Diverse data-driven models have been proposed to characterize some antenna response metrics, such as gain or directivity, reflection coefficient, bandwidth, resonant frequency, etc., in the presence of multiple random disturbances. These models include polynomial chaos expansion [3-6], heuristic algorithms [7-9], and response feature approximation [10-11]. In recent years, there has been a growing focus on accurately modeling the complete far-field radiation, including both the amplitude and phase of the electric field $\boldsymbol{E}$. This is particularly needed in ultra-wideband or MIMO scenarios. Rossi [12] introduced a stochastic collocation model for the electric field. The field is parsimoniously parametrized using vector spherical harmonic (VSH) coefficients which are then approximated using generalized polynomial chaos expansion (gPCE). In a separate study, our team proposed an iterative process that combines dominant VSH modes selection and the least-angle regression sampling (LARS) -based PCE [13] to extract efficient surrogate models [14-15]. This approach improves modeling efficiency for high-dimensional cases and extents to cover a continuous operating frequency range. Hu [16] proposed a general framework for building surrogate models for the electric field amplitude $|\boldsymbol{E}|$. They employed dynamic LARS to select the most relevant input parameters before constructing an artificial neural network-based model. This framework demonstrated high efficiency with limited training data.

To date, a major challenge for complete far-field modeling that has not been fully addressed is the multilevel random effects caused by random disturbances. We can distinct the "*global*" effect which occurs as an overall contraction of the radiation pattern, and the "*fine*" effect which occurs as the distortion (or reshaping) of the radiation pattern. Essentially, the *global* effect is due to the decrease in matching efficiency caused by detuning or mismatching phenomena, whereas the *fine* effect reflects the redistribution of radiated power between the various VSH modes. The contribution of the *global* effect to the total uncertainty in far-field radiation can be two orders of magnitude higher than that of the *fine* effect, but it's also essential to characterize the latter accurately, not least because it has a non-negligible impact on the phase of the field. Multilevel effects considerably hinder the model convergence and require a large training dataset to achieve satisfactory accuracy, thus

Manuscript resubmitted May 11, 2024. This work was supported in part by the National Natural Science Foundation of China under Grants 61901253, 61771300, and in part by the Aeronautical Science Foundation of China under grant 202000460S6001. (*Corresponding author: Jinxin Du*)

Jinxin Du and Ruimeng Wang are with the Sino-European School of Technology, Shanghai University, Shanghai 200444, China (email: jinxin_du@shu.edu.cn, wrm981223@163.com).

Christophe Roblin is with the LTCI, Télécom Paris, Institut Polytechnique de Paris, 91120 Palaiseau, France (email: christophe.roblin@telecom-paris.fr).

Xue-Xia Yang is with the Key Laboratory of Specialty Fiber Optics and Optical Access Networks, Shanghai University, Shanghai 200444, China (email: yang.xx@shu.edu.cn).

Bin Han is with the Division of Wireless Communications and Radio Positioning (WiCoN), RPTU Kaiserslautern-Landau, 67663 Kaiserslautern, Germany (email: bin.han@rptu.de).

leading to high computational cost.

We present in this paper a new approach to effectively deal with multilevel random effects on the antenna far-field. *Global* random effect due to detuning (or mismatching) and *fine* random effect representing power redistribution will be tackled separately. The key point is to emphasize that detuning information is essentially contained in the reflection coefficient $S_{11}(f)$. Therefore, instead of directly modeling the complete far-field, we can build separately two "nested" sub-models: one to characterize the far-field modified by a desensitization technique to detuning, and the other to characterize the reflection coefficient $S_{11}(f)$. A centering technique based on cross-correlation is proposed to gather all random $S_{11}(f)$ curves around a reference location to largely reduce the non-linearity of the problem. Finally, the complete far-field model is obtained by combining the two sub-models. This new approach avoids dealing with multilevel random effects at one single stage, which speeds up model convergence, improves the robustness of the surrogate model, and allows some generalization of stochastic modeling to a wider variety of applications.

The paper is organized as follows: in Section II, the principle of the PCE-based stochastic modeling methodology and the multilevel random effects separation technique are outlined; in Section III, verification is carried out on a wearable textile patch antenna and comparative results are discussed; general conclusions and perspectives are drawn in Section IV.

II. Modeling of the Complete Far-Field Radiation

A. Formulation of the Problem

A flexible antenna subjected to random disturbances can be regarded as a "Blackbox"-like uncertain system, whose input is a multi-dimensional random variable $\boldsymbol{X} = (X_1, X_2, ...)^T$ and the output of interest is the electric far-field $\mathbf{E}^{\infty}(f, \hat{\mathbf{r}})$. We denoted the output perturbed by the input as $\mathbf{E}^{\infty}(\boldsymbol{X}, f, \hat{\mathbf{r}})$, which is represented here by the Antenna Transfer Function (ATF) $\mathcal{H}(\boldsymbol{X}, f, \hat{\mathbf{r}})$, defined in [17] as:

$$\mathcal{H}(\boldsymbol{X}, f, \hat{\mathbf{r}}) \triangleq \frac{r e^{jkr}}{a_1(f)} \sqrt{\frac{4\pi}{\eta_0}} \cdot \mathbf{E}^{\infty}(\boldsymbol{X}, f, \mathbf{r}) \tag{1}$$

where a_1 is the incident partial wave (unit is $\sqrt{Watt}$) measured in the input plane of the antenna, $\hat{\mathbf{r}} = (\theta, \varphi)$ the unit radial vector (the spherical angle couple, in the arguments of the functions), j the imaginary unit ($j^2 = -1$), k the wavenumber, $f \in [f_{\min}, f_{\max}]$ the considered frequency, and $\mathbf{E}^{\infty}(\boldsymbol{X}, f, \hat{\mathbf{r}})$ the radiated far-field. This ATF is in fact a *realized* transfer function, because the chosen normalization leads to the realized gain, i.e., $\|\mathcal{H}(f, \hat{\mathbf{r}})\|^2 = G_r(f, \hat{\mathbf{r}})$. Therefore, it accounts for both the matching and directional characteristics of the antenna.

To quantitatively characterize the ATF over a considered frequency range, we take the simplifying assumption that treats the *deterministic* frequency parameter "f" as an ordinary *random* variable, so that we can take the vector space generated by the random variables $(X_1, X_2, \ldots, f)^T$ as the input space for this stochastic process. Sophisticated approaches like PCE and its variants can be used to obtain closed-form solutions. As mentioned previously, multilevel random effects aggravate the problem of the curse of dimensionality and non-linearities. It is thereby necessary to develop large experimental designs (EDs) with enormous training data, entailing high computational cost.

B. Detuning-Desensitized Antenna Transfer Function

To alleviate the challenge of multilevel random effects, we propose to characterize the *global* and *fine* effect separately. This is achieved by "decoupling" the detuning phenomenon from the ATF. Seeing that the detuning effect is mainly contained in the reflection coefficient, it amounts to construct a new detuning-desensitized ATF $\tilde{\mathcal{H}}(\boldsymbol{X}, f, \hat{\mathbf{r}})$ as (2):

$$\tilde{\mathcal{H}}(\boldsymbol{X}, f, \hat{\mathbf{r}}) \triangleq \frac{\mathcal{H}(\boldsymbol{X}, f, \hat{\mathbf{r}})}{\sqrt{1 - |S_{11}(\boldsymbol{X}, f)|^2}} \tag{2}$$

where $S_{11}(\boldsymbol{X}, f)$ is the reflection coefficient of the $\boldsymbol{X}$-perturbed antenna. The matching efficiency is $\eta_m = (1 - |S_{11}|^2)$, thereby,

$$\|\tilde{\mathcal{H}}(\boldsymbol{X}, f, \hat{\mathbf{r}})\|^2 = \frac{\|\mathcal{H}(\boldsymbol{X}, f, \hat{\mathbf{r}})\|^2}{\eta_m} = \frac{G_r(\boldsymbol{X}, f, \hat{\mathbf{r}})}{\eta_m} = G(\boldsymbol{X}, f, \hat{\mathbf{r}}) \tag{3}$$

where G and G_r are respectively the power and realized gains of the antenna. Note that the definition of $\tilde{\mathcal{H}}$ is the same as that of the "*phasor*" $\hat{\mathbf{g}}$ proposed in [18].

Physically, $\tilde{\mathcal{H}}$ represents the ATF as if the antenna were always in perfect impedance match with the feeding line, regardless of the presence of input disturbances or frequency sweep. It is therefore, in a way, much more "insensitive" to the detuning effect. Next, it is easier to construct sub-models for both the desensitized ATF and the reflection coefficient separately. Thereby, the overall modeling process converges faster, resulting in a more robust model.

C. Stochastic Modeling of the Detuning-Desensitized ATF

Let there be M–1 random variables with a known joint probability distribution function (PDF). Additionally, consider the frequency "f" as an extra *random* variable with the same type of marginal PDF. We adopt the PCE method described in [14] to construct a surrogate model that maps $\tilde{\mathcal{H}}(\boldsymbol{X}, f, \hat{\mathbf{r}})$ to $(\boldsymbol{X}, f)$. The construction process of the surrogate model involves two main steps. Firstly, the desensitized ATF is parsimoniously represented by a limited number of energetically dominant VSH modes; secondly, each selected VSH mode is decomposed into a weighted sum of chaos polynomial depending on the input variables, using the LARS-PCE algorithm. The accuracy of the surrogate model can be progressively improved through an iterative procedure by enriching the ED. The final surrogate model, denoted as $\hat{\tilde{\mathcal{H}}}(\boldsymbol{X}, f, \hat{\mathbf{r}})$ reads (4),

$$\hat{\tilde{\mathcal{H}}}(\boldsymbol{X}, f, \hat{\mathbf{r}}) = j \sum_{q=1}^{Q} \sum_{\boldsymbol{\alpha} \in \mathbb{N}^M}^{|\boldsymbol{\alpha}|_1 \le N_{\mathrm{PCE}}} (-j)^{\mathrm{mod}(q,\,2)}\, y_{\boldsymbol{\alpha}}^{q}\, \Phi_{\boldsymbol{\alpha}}(\boldsymbol{X}, f)\, \hat{\boldsymbol{\psi}}_{\lceil q/2 \rceil}(\hat{\mathbf{r}}) \tag{4}$$

where $\{\hat{\boldsymbol{\psi}}_q(\hat{\mathbf{r}})\}$ is an orthonormal basis in the L^2 space of spherical harmonics; $\{\Phi_{\boldsymbol{\alpha}}(\boldsymbol{X})\}$ is a multivariate orthonormal basis in the Hilbert space $L^2_{P_X}(\mathbb{R}^M, \mathbb{R})$ with respect to the inner product $< u, v > = \int_{\mathbb{R}^M} u(\boldsymbol{x}) v(\boldsymbol{x}) f_X(\boldsymbol{x}) d\boldsymbol{x}$; $\{y_{\boldsymbol{\alpha}}^q\}$ are the unknown scalar coefficients to be resolved during the modeling process. (*Please refer to [14] for more details.*)

D. Stochastic Modeling of the Reflection Coefficient $S_{11}(f)$

The modeling of the frequency response $S_{11}(\boldsymbol{X}, f)$ involves two successive steps. Firstly, we employ a reduction order method based on Fourier series expansion (FSE) to parsimoniously represent $S_{11}(f)$. Subsequently, we utilize LARS-PCE to decompose each Fourier coefficient into chaos polynomials of the input parameters. Various approaches, such as polynomial fitting, Gaussian fitting [19], transfer function identification [20], and FSE, can be employed to compress a frequency response function. We have opted for FSE to characterize the real and imaginary components of $S_{11}(f)$ because they closely resemble the composition of harmonics.

In most cases, the phenomenon of detuning due to structural variability appears, to a 1st approximation, as a translation of the frequency response (with respect to the nominal response) of each random antenna realization. Compensating for these translation differences before modeling is of crucial importance to reduce the variation range of the random system. It is the key step in accelerating the convergence of the modeling process and improving model accuracy. We first perform a translation operation on the reflection coefficient curves to "center" or "align" them to some extent around a reference curve, as shown in Fig. 1 and denoted as in (5):

$$\bar{S}_{11}(\boldsymbol{X}, f) = S_{11}(\boldsymbol{X}, f - \Delta f(\boldsymbol{X})) \tag{5}$$

where $\Delta f(\boldsymbol{X})$ is the frequency offset of the $\boldsymbol{X}$-disturbed reflection coefficient curve with respect to the reference curve. It can be determined as the lag when performing the cross-correlation between these two curves [21].

Next, we proceed to extract the representative features of the "centered" reflection coefficients which are now much less sensitive to the random input $\boldsymbol{X}$, utilizing the FSE:

$$\bar{S}_{11}^{R,I}(\boldsymbol{X}, f) = a_0^{R,I}(\boldsymbol{X}) + \sum_{k=1}^{n} a_k^{R,I}(\boldsymbol{X})\cos(k\tau(\boldsymbol{X})f) + b_k^{R,I}(\boldsymbol{X})\sin(k\tau(\boldsymbol{X})f) \tag{6}$$

where $\bar{S}_{11}^{R/I}$ is the real or imaginary part of the $\boldsymbol{X}$-disturbed centered reflection coefficient, n is the order of the truncated expansion, a_k and b_k are coefficients of the *k-th* order components, and τ is the variable (in seconds) in the dual space, considered here as a representative parameter of the model.

Both the coefficients $\{a_0(\boldsymbol{X}), a_1(\boldsymbol{X}), b_1(\boldsymbol{X}), \cdots, \tau(\boldsymbol{X})\}$ and the frequency offset $\Delta f(\boldsymbol{X})$ can be each stochastically modeled using the LARS-PCE algorithm, resulting in a series of models, denoted as $\{\hat{a}_0(\boldsymbol{X}), \hat{a}_1(\boldsymbol{X}), \hat{b}_1(\boldsymbol{X}), \cdots, \hat{\tau}(\boldsymbol{X})\}$ and $\Delta f(\boldsymbol{X})$.

For any new input $\boldsymbol{X}$, the surrogate model predicts the reflection coefficient $\hat{S}_{11}(\boldsymbol{X}, f)$ of the corresponding antenna as in (7). Finally, the surrogate model $\hat{\boldsymbol{\mathcal{H}}}(\boldsymbol{X}, f, \hat{\mathbf{r}})$ for the complete far-field can be obtained by combining (4), (7) and (8).

$$\begin{cases} \hat{S}_{11}(\boldsymbol{X}, f) = \hat{\bar{S}}_{11}(\boldsymbol{X}, f + \Delta f(\boldsymbol{X})) \\ \hat{\bar{S}}_{11}(\boldsymbol{X}, f) = \hat{a}_0(\boldsymbol{X}) + \sum_{k=1}^{n} \hat{a}_k(\boldsymbol{X})\cos(k\hat{\tau}(\boldsymbol{X})f) + \hat{b}_k(\boldsymbol{X})\sin(k\hat{\tau}(\boldsymbol{X})f) \end{cases} \tag{7}$$

$$\hat{\boldsymbol{\mathcal{H}}}(\boldsymbol{X}, f, \hat{\mathbf{r}}) = \hat{\bar{\boldsymbol{\mathcal{H}}}}(\boldsymbol{X}, f, \hat{\mathbf{r}}) \times \sqrt{1 - \left|\hat{S}_{11}(\boldsymbol{X}, f)\right|^2} \tag{8}$$

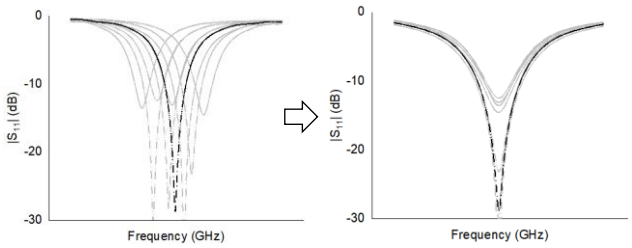

Fig. 1. The reflection coefficient curves: (a) before and (b) after centering.

TABLE I DESIGN PARAMETERS OF THE TEXTILE PATCH AND A PHOTO

Random parameter	Unit	Nominal value	Support
κ	mm^{-1}	0	[0, 1/30]
C	mm	0	[0, 5]
s	-	1	[1, 1/0.6]
ε_r	-	1.776	[1.6, 1.9]
f	GHz	2.45	[2.4, 2.5]

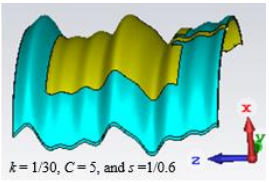

III. APPLICATION TO A TEXTILE PATCH ANTENNA

The proposed modeling approach was applied to a flexible textile patch antenna described in [14] for uncertainty quantification. Its performance, with regards to modeling efficiency, model accuracy, and robustness, has been verified by comparing with the LARS-PCE method in [14], which did not specifically address the issue of multilevel random effects.

A. Flexible Patch Antenna

The antenna is a classic microstrip-fed rectangular patch antenna. It consists of two layers of copper foil and one layer of jean tissue (with a relative permittivity of 1.776 and a loss tangent of 0.05). In this work, we consider bending and crumpling deformations, as well as variations in the relative permittivity of the dielectric layer. The geometric, electromagnetic, and frequency parameters are assumed as mutually independent and uniformly distributed random variables, as detailed in Table I, where κ represents the curvature of the substrate along the long side of the patch; C and s are the amplitude and the spatial pseudo-frequency that characterize the "*Weierstrass* fractal shape" modeling crumpling along the long side; the variation in ε_r can be attributed to manufacturing tolerances, temperature or humidity instability in the environment; and the frequency range is simply the passband of the antenna.

B. Detuning-Desensitized ATF Modeling

Following the procedure outlined in section II.C, we derived a series of surrogate models for the desensitized ATF $\tilde{\boldsymbol{\mathcal{H}}}(\boldsymbol{X}, f, \hat{\mathbf{r}})$ as the ED size gradually increases. To assess the predictive accuracy of these surrogate models, we employed a cross-validation metric called the weighted leave-one-out error, denoted as e_{WTLOO} (defined in [14]). Empirically, a value of $e_{\mathrm{WTLOO}} \leqslant 5\%$ guarantees relatively good accuracy.

For comparison, Fig. 2 depicts, with a black curve, the same metric for the surrogate models of the direct complete ATF. These models were built using the same LARS-PCE algorithm and the same ED as that used for the desensitized ATF models. As expected, the error decreases with increasing ED size in both cases. However, in terms of convergence,

TABLE II COMPARISON OF DIFFERENT SURROGATE MODELS

Surrogate model		Cardinal of ED	Accuracy of the surrogate model (test on an independent random test set with 2000 cases)				
			Distribution of the prediction errors e_{sup} (dB)			Average prediction error (dB)	Max prediction error (dB)
			Low (≤ 1)	Medium (1 – 1.5)	High (1.5 – 2.5)		
Ref. [14]	*Model1_700*	700	89.32%	8.16%	2.52%	0.53	2.2
this work	*Model2_300*	300	89.76%	8.37%	1.87%	0.56	3.04
this work	*Model2_700*	700	96.02%	3.68%	0.30%	0.43	2.28

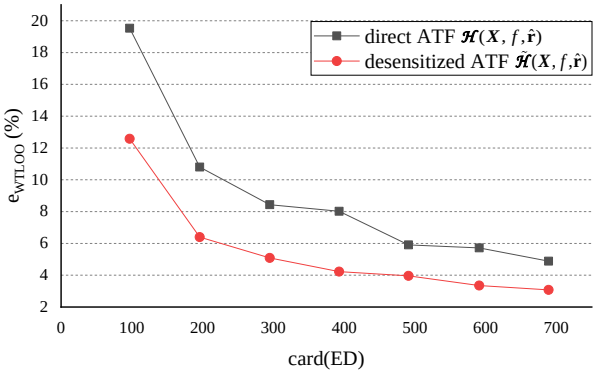

Fig. 2. Prediction error of surrogate models adaptively constructed by enriching the ED.

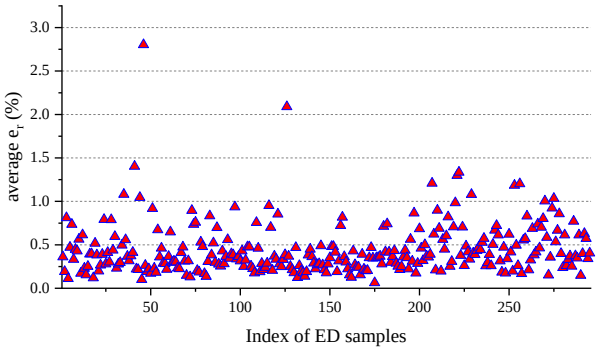

Fig. 3. Relative error of the constructed surrogate model for S_{11}.

the red curve outperforms the black curve. When all 700 realizations of the ED are used as the training dataset, the prediction error in the 1st case (red curve) is significantly lower than in the second (black curve), i.e., 3.1 % vs 5 %. Similarly, to achieve the criterion $e_{WTLOO} \leqslant 5$ %, only 300 realizations are needed for the 1st case, whereas 700 realizations are required for the 2nd case. It is essential to emphasize that the acquisition of the ED databases using full-wave electromagnetic simulations is the most time-consuming step (i.e., about 15 minutes per simulation). This new approach thereby reduces the total cost of modeling by almost 57 % (i.e., about 100 hours in total).

By adopting the modeling procedure described in section II.D, we derived a surrogate model for the reflection coefficient $S_{11}(\boldsymbol{X}, f)$ based on the first 300 ED realizations. To quantify the accuracy of the surrogate model, we define a new metric e_m that represents the relative error between the matching efficiencies η_m of the original and model-reconstructed $S_{11}(f)$. We further define its average value over the considered frequency range as in (9) to account for the overall performance. Fig. 3 shows the relative error remains below 3 % for all ED realizations.

$$\begin{cases} e_m(f) = \dfrac{\eta_m(f) - (\eta_m(f))_{rcs}}{\eta_m(f)} \times 100\% \\ \bar{e}_m = \underset{f \in [2.4,\ 2.5]}{aver} [e_m(f)] \end{cases} \tag{9}$$

C. Complete Surrogate Model for Far-Field Radiation

By combining the two sub-models presented (of the desensitized ATF and the S_{11}), we finally obtain a surrogate model for the complete ATF, which represents far-field radiation, as defined in (8). Let's refer to the surrogate models constructed by using the original methodology from [14] as "*Model1_700*" (i.e., derived from 700 ED realizations), and by using our Two-step method in this work as "*Model2_300*" (i.e., derived from 300 ED realizations) and "*Model2_700*" (i.e., derived from 700 ED realizations). To verify the prediction capabilities, we tested them over an independent random test set comprising 2000 realizations. We compared the ATFs computed with the surrogate models to those directly obtained from the EM simulations (which are used as a reference).

Table II summarizes the prediction error e_{sup} for different surrogate models. e_{sup} indicates the maximal absolute difference between the model-predicted and the original ATFs in terms of the realized gain G_r in a *10dB-drop* solid angle that encompasses most of the broadside hemisphere (please refer to [14]). In order to show the distribution of the prediction errors, we classified them into three categories: "Low error level" ($e_{Sup} \leq 1$ dB), "Medium error level" ($1 < e_{Sup} \leq 1.5$ dB), and "High error level" ($1.5 < e_{Sup} \leq 2.5$ dB). The average and maximal prediction error over the 2000 cases are also given. It is noteworthy that *Model2_300* exhibits a prediction error level similar to *Model1_700*, but requires 57 % less computational cost. Conversely, *Model2_700* incurs the same cost as *Model1_700*, but has significantly improved performance. Notably, the percentage of cases falling into the "Low error level" category has increased from 89.32 % to 96.02 %, and the percentage of cases categorized as "High error level" has sharply decreased from 2.52 % to only 0.3 %.

IV. CONCLUSION

Multilevel random effects can intensively hinder the antenna modeling convergence. In this work, we introduce a novel technique to separately characterize the *global* effect mainly induced by detuning (or mismatch) phenomenon and the *fine* effect related to antenna directional characteristics. Application to a textile patch antenna shows the proposed methodology could significantly enhance the convergence rate of the modeling process, leading to a substantial reduction in modeling cost. Such surrogate models can be beneficial for uncertainty quantification of a radio link in WBAN scenarios (particularly for broadside off-body communications), and for irregular array synthesis and MIMO systems evaluation.

REFERENCES

[1] K. N. Paracha, S. K. A. Rahim, P. J. Soh, and M. Khalily, "Wearable antennas: A review of materials, structures, and innovative features for autonomous communication and sensing," *IEEE Access*, vol. 7, pp. 56694-56712, 2019.

[2] U. Ali, S. Ullah, B. Kamal, L. Matekovits, and A. Altaf, "Design, Analysis and Applications of Wearable Antennas: A Review," *IEEE Access*, 2023.

[3] F. Boeykens, H. Rogier, and L. Vallozzi, "An efficient technique based on polynomial chaos to model the uncertainty in the resonance frequency of textile antennas due to bending," *IEEE Transactions on Antennas and Propagation*, vol. 62, no. 3, pp. 1253-1260, 2014.

[4] M. Rossi, A. Dierck, H. Rogier, and D. Vande Ginste, "A stochastic framework for the variability analysis of textile antennas," *IEEE Transactions on Antennas and Propagation*, vol. 62, no. 12, pp. 6510-6514, 2014.

[5] M. Rossi, S. Agneessens, H. Rogier, and D. Ginste, "Stochastic analysis of the impact of substrate compression on the performance of textile antennas," *IEEE Transactions on Antennas and Propagation*, vol. 64, no. 6, pp. 2507-2512, 2016.

[6] H. Rogier, "Generalized Gamma-Laguerre Polynomial Chaos to Model Random Bending of Wearable Antennas, " *IEEE Antennas and Wireless Propagation Letters*, vol. 21, no. 6, pp. 1243-1247, 2022.

[7] J. Dong, W. Qin, and M. Wang, "Fast Multi-Objective Optimization of Multi-Parameter Antenna Structures Based on Improved BPNN Surrogate Model, " *IEEE Access*, vol. 7, pp. 77692-77701, 2019.

[8] L. Yuan, X. S. Yang, C. Wang, and B. Z. Wang, "Multibranch Artificial Neural Network Modeling for Inverse Estimation of Antenna Array Directivity," *IEEE Transactions on Antennas and Propagation*, vol. 68, no. 6, pp. 4417-4427, 2020.

[9] K. Fu, X. Cai, B. Yuan, Y. Yang, and X. Yao, "An Efficient Surrogate Assisted Particle Swarm Optimization for Antenna Synthesis," *IEEE Transactions on Antennas and Propagation*, vol. 70, no. 7, pp. 4977-4984, 2022.

[10] S. Koziel and A. Pietrenko-Dabrowska, "Tolerance Optimization of Antenna Structures by Means of Response Feature Surrogates, " *IEEE Transactions on Antennas and Propagation*, vol. 70, no. 11, pp. 10988-10997, 2022.

[11] A. Pietrenko-Dabrowska and S. Koziel, "Accelerated Parameter Tuning of Antenna Structures by Means of Response Features and Principal Directions," *IEEE Transactions on Antennas and Propagation*, vol. 71, no. 11, pp. 8987-8999, 2023.

[12] M. Rossi, G. J. Stockman, H. Rogier, and D. Vande Ginste, "Stochastic analysis of the efficiency of a wireless power transfer system subject to antenna variability and position uncertainties," *Sensors*, vol. 16, no. 7, 2016.

[13] G. Blatman and B. Sudret, "Adaptive sparse polynomial chaos expansion based on least angle regression," *Journal of Computational Physics*, vol. 230, no. 6, pp. 2345-2367, 2011.

[14] J. Du and C. Roblin, "Stochastic surrogate models of deformable antennas based on vector spherical harmonics and polynomial chaos expansions: application to textile antennas," *IEEE Transactions on Antennas and Propagation*, vol. 66, no. 7, pp. 3610-3622, 2018.

[15] J. Du and C. Roblin, "Statistical modeling of disturbed antennas based on the polynomial chaos expansion," *IEEE Antennas and Wireless Propagation Letters*, vol. 16, no. 1, pp. 1843-1846, 2016.

[16] Runze Hu, Vikass Monebhurrun, Ryutaro Himeno, Hideo Yokota, and Fumie Costen, "A General Framework for Building Surrogate Models for Uncertainty Quantification in Computational Electromagnetics," *IEEE Transactions on Antennas and Propagation*, vol. 70, no. 2, pp. 1402-1414, 2022.

[17] C. Roblin, S. Bories, and A. Sibille, "Characterization tools of antennas in the Time Domain," in *International Workshop on UWB Systems, IWUWBS*, Oulu, June 2003.

[18] O. Franek, "Phasor Alternatives to Friis' Transmission Equation," *IEEE Antennas and Wireless Propagation Letters*, vol. 17, no. 1, pp. 90-93, 2018.

[19] Y. Kim, S. Keely, J. Ghosh, and H. Ling, "Application of artificial neural networks to broadband antenna design based on a parametric frequency model," *IEEE Transactions on Antennas and Propagation*, vol. 55, no. 3, pp. 669-674, 2007.

[20] J. Du and C. Roblin, "Statistical modeling of the reflection coefficient of deformable antennas," in *EuCAP*, Paris, France, March 2017.

[21] https://www.mathworks.com/help/matlab/ref/xcorr.html